

Convex Geometric Motion Planning on Lie Groups via Moment Relaxation

Sangli Teng, Ashkan Jasour, Ram Vasudevan, Maani Ghaffari

Abstract—This paper reports a novel result: with proper robot models on matrix Lie groups, one can formulate the kinodynamic motion planning problem for rigid body systems as *exact* polynomial optimization problems that can be relaxed as semidefinite programming (SDP). Due to the nonlinear rigid body dynamics, the motion planning problem for rigid body systems is nonconvex. Existing global optimization-based methods do not properly deal with the configuration space of the 3D rigid body; thus, they do not scale well to long-horizon planning problems. We use Lie groups as the configuration space in our formulation and apply the variational integrator to formulate the forced rigid body systems as quadratic polynomials. Then we leverage Lasserre’s hierarchy to obtain the globally optimal solution via SDP. By constructing the motion planning problem in a sparse manner, the results show that the proposed algorithm has *linear* complexity with respect to the planning horizon. This paper demonstrates the proposed method can provide rank-one optimal solutions at relaxation order two for most of the testing cases of 1) 3D drone landing using the full dynamics model and 2) inverse kinematics for serial manipulators.

I. INTRODUCTION

The kinodynamic motion planning [1], or trajectory optimization [2], which aims to synthesize robot motion subject to kinematics, dynamics, and input constraints, is fundamental in robotics research. A typical formulation of kinodynamic motion planning is a constrained optimization problem, usually nonconvex due to the nonlinear dynamics and obstacle configurations. Despite the nonconvexity of these problems, the optimization methods that exploit the local gradient information have been successfully applied to find local solutions. Unless problem-specific convexification is accessible [3], there is generally no guarantee on the global optimality

Indeed, the complexity of motion planning problems with arbitrary obstacles is high [4–6] that one should not expect an efficient algorithm for general problems. For motion planning problems in moderate size, global optimization techniques, such as mixed integer programming [7–13] and polynomial optimization [14–16], have been applied to obtain or approximate the globally optimal solutions. However, these methods do not consider robot dynamics or apply approximations that would sacrifice the modeling fidelity. For motion planning using full robot dynamics, such engineering compromise would limit the potential of the robots.

Thus, the natural question is how can we obtain the *globally optimal* solution of motion planning problem at the dynamics

S. Teng, R. Vasudevan, and M. Ghaffari are with the University of Michigan, Ann Arbor, MI 48109, USA. {sanglit, ramv, maanigj}@umich.edu

A. Jasour is with Team 347T-Robotic Aerial Mobility, Jet Propulsion Lab, Pasadena, CA, 91109. jasour@jpl.caltech.edu

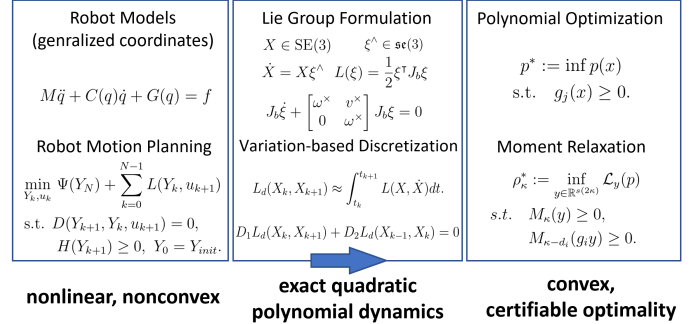


Fig. 1: The proposed geometric motion planning framework on Lie group. The motion planning problem is usually nonconvex due to the nonlinear dynamics. By utilizing robot models on Lie group and variation-based discretization, the motion planning problem can be converted to *exact* quadratic polynomial optimization problem (POP). Via the moment relaxation method, i.e., Lasserre’s hierarchy, the POP can be solved by a sequence of SDPs. We show that in our case, the second-order relaxation successfully provides certified globally optimal solutions for most of the testing cases despite the numerical challenges.

level using *exact* models? The main challenges are the scalability of the global optimization algorithm and the absence of proper robot formulations. For the former problem, recent progress in the Polynomial Optimization Problem (POP), i.e., Lasserre’s hierarchy [17, 18], enables one to compute globally optimal solutions of POPs via a sequence of Semidefinite Programming (SDP) that can be solved in polynomial time. For the latter problem, we introduce the Lie group-based formulation for robots composed of rigid bodies.

In this paper, we show that bridging the geometric robotics formulation and Lasserre’s hierarchy leads to certifiably optimal solutions for motion planning problems using the full dynamics model. We exploit the property of the configuration space of rigid body dynamics and apply variational integrator [19] on Lie groups to generate an exact polynomial formulation. Then we formulate the kinodynamic motion planning problem as a sparse POP with only quadratic polynomials. We further leverage Lasserre’s hierarchy to approximate the globally optimal solutions. The main contributions of this paper are summarized as follows.

- 1) Derivation of robotics dynamics model on matrix Lie groups using the variational integrator in discrete time. We show that the forced rigid body system can be represented by *exact* quadratic polynomials.
- 2) Formulation of kinodynamic motion planning problem as a low-order and sparse POP that can be solved via SDP at finite relaxation order. We show that the proposed formulation has linear time complexity with respect to the planning horizon.

- 3) Evaluations of the proposed algorithms on 3D inverse kinematics for serial manipulators and trajectory planning for 3D drone using full dynamics model. We show that the second-order moment relaxations provide rank-one globally optimal solutions or provide infeasibility certificates for most of the testing cases modulo some numerical issues of the SDP solver.

II. RELATED WORK

A. Sampling-based motion planning

The sampling-based motion planning algorithm has gained success in recent decades [20–26]. These sampling-based methods are complete (or, resp. optimal), in the sense that the probability of finding the solution (or, resp. finding the optimal solution) converges to one when the sampling is enough [23, 27]. However, as the completeness of these methods is only in the sense of probability, there is no guarantee of the runtime, and the algorithm may run forever if the solution does not exist. Due to the sampling nature of these algorithms, the solutions are chattering that need refining by local solvers.

B. Global optimization-based motion planning

The mixed integer programming has been applied to the collision avoidance or path planning problem for aerial [7], or ground vehicles [8, 9], and legged robot [10–12]. The work of [7–9] aims at path planning that omits the dynamics of the robots. The work of [10–12] applied simplified dynamics models for legged robot step planning. These methods are based on simplified models, specifically for legged robots, and do not consider the 3D kinematics or dynamics constraints. Research [13] represents the $SO(3)$ surface by the convex hull in partitioned intervals, thus making the Inverse Kinematics (IK) problem a mixed-integer convex optimization. Then the branch-and-bound process [28] is applied to solve the mixed-integer convex optimization. High accuracy approximation of the $SO(3)$ would require more intervals that dramatically increase the runtime. These combinatorial methods are complete and capable of obtaining the globally optimal solutions [27], while the cost is the exponential time complexity and omission of the geometry of the configuration space. The combinatorial methods cannot scale well for long-horizon planning and complex rigid body configurations.

Piece-wise linear kinematics model and Lasserre’s hierarchy are applied in [14] to plan paths with collisions defined by time-varying polynomial inequalities. With the increase of moment relaxation order, research [14] could asymptotically find the collision-free path when a moving obstacle is presented. Research [29] extends such Lasserre’s hierarchy-based method to develop risk-bounded trajectory planners in the presence of uncertain time-varying obstacles using the notion of risk contours [30]. Moment relaxation methods have been applied to optimal control of hybrid systems [31] in continuous time. Via a sequence of SDPs, the control input and state monotonically converge to the global optimum. Sum-of-squares programming has been applied in [32] to verify the region of attraction for the feedback controller. Both [31] and

[32] consider Taylor expansions to approximate the nonlinear robot dynamics. As the Taylor expansion is an infinite series, finite order approximation can not be exact, and higher order approximation inevitably increases the size of the higher-order moment matrix.

Trigonometric functions have been represented as rational functions in [15, 16] to formulate the kinematic constraints in the IK problem. Using this parameterization, [16] applies the Lasserre’s hierarchy to compute globally optimal solutions of IK and [15] apply the sum-of-squares [33, 34] to certify the collision-free regions. However, both [15] and [16] only consider the rotation about a single axis and need to represent the joint $SE(3)$ pose by a chain of trigonometric polynomials. The drawback is that when the kinematic chain increases, the degree of the polynomial representing the pose also increases. Additionally, [15, 16] are dense formulations as each equality constraint involves all joint angles. The work of [35] casts the IK as a problem of finding the nearest point of an algebraic variety and proves all non-singular poses can be tightly solved by sparse SDP relaxation [36]. However, this formulation relies on distance geometry that only applies to kinematic problems. The work of [37, 38] describe the exact uncertainty propagation of systems parameterized by trigonometric polynomials using the notion of trigonometric moments. Though dynamics models are considered in both cases, the constraints between the Euler angles and their trigonometric functions are not linear. Such constraints make it hard to lift the dynamics constraints to the moment space. To solve the above issues, our geometric-based formulation is sparse and only involves quadratic polynomials that can be applied for long-horizon applications.

C. Lasserre’s Hierarchy and certifiable optimality

Lasserre’s hierarchy converts the POP to infinite dimensional linear programming in measure space and approximates the global solution via truncated moment sequences in finite dimension [17, 18]. By increasing the order of the moment matrix, one can monotonically approximate the globally optimal solution of POP by solving a sequence of SDPs. When the cost function and constraints satisfy certain technical conditions [39], Lasserre’s hierarchy can converge *exactly* to the global optimum in finite relaxation order. For large-scale problems, the sparsity pattern in POP has been used to reduce the size of the SDP by breaking the dense moment matrix into smaller ones [40–42]. For control problems that satisfy Markov assumption, the sparsity pattern [41, 43] makes the computation time linear in the problem horizon [42].

Lasserre’s hierarchy has been applied to perception problem [44] as the certifiable algorithm [45]. The certifiable algorithm [44, 45] requires that: (i) the algorithm runs in polynomial time, (ii) returns a globally optimal solution with a certificate of the optimality, (iii) or fails to do so but provides a bound on the objective value. When the relaxation order of Lasserre’s hierarchy is determined, the SDP can be solved in polynomial time. The optimum of SDP can also be certified as the globally optimal solution via rank conditions of the moment

matrix or serve as a lower bound estimation for the problem [18]. Such properties are rarely seen in the existing motion planning algorithms based on sampling, combinatorial solvers, or nonlinear local solvers.

Continuous time control problems of polynomial systems have been lifted to space of measure to obtain optimal feedback [31, 46–48], region of attraction [49] or backward reachable set [50]. Though asymptotically convergent approximation by Lasserre’s hierarchy is guaranteed, finite convergence is not observed in these cases. In this work, we leverage Lasserre’s hierarchy by converting the discrete-time motion planning problem to exact POP for a single trajectory. We find that our numerical simulations can certify the optimal solution at the second relaxation order.

III. BACKGROUND AND PRELIMINARY RESULTS

A. Polynomial optimization and Lasserre’s Hierarchy

Let $\mathbb{R}[x]$ be the ring of polynomial with real coefficients and $x := (x_1, x_2, \dots, x_n)$. Given an integer r , we define the set $\mathbb{N}_r^n := \{\alpha \in \mathbb{N}^n \mid \sum_i \alpha_i \leq r\}$. The monomial with degree up to r can be defined as $x^\alpha := x_1^{\alpha_1} x_2^{\alpha_2} \dots x_n^{\alpha_n}$, $\alpha \in \mathbb{N}_r^n$, and we have the canonical basis for polynomial degree up to r :

$$v_r(x) := (1, x_1, x_2, \dots, x_n, x_1^2, x_1 x_2, \dots, x_n^2, x_1^r, x_2^r, \dots, x_n^r). \quad (1)$$

Let $s(r) := \binom{n+r}{n}$ be the dimension of $v_r(x)$. Then any r -degree polynomial $p(x) : \mathbb{R}^n \rightarrow \mathbb{R}$ could be expressed as:

$$p(x) = \sum_{\alpha} p_{\alpha} x^{\alpha} = \langle p, v_r(x) \rangle, \quad (2)$$

where $p = \{p_{\alpha}\}$ denotes the coefficients corresponding to the basis defined in (1). We define the POP as follows.

Problem 1 (Polynomial Optimization Problem).

$$\begin{aligned} p^* &:= \inf p(x) \\ \text{s.t. } &g_j(x) \geq 0, \quad \forall j \in \{1, \dots, m\}. \end{aligned} \quad (\text{POP})$$

where p, g_j are polynomials. We denote the feasible set as \mathbb{K} .

We denote the degree, i.e., the highest order of monomial, of polynomial g as $\deg g$. Then we have the degree integers as $d_i := \lceil \deg(g_i)/2 \rceil$ and $d_g = \max\{1, d_1, \dots, d_m\}$, where $\lceil a \rceil$ denotes the integer greater than or equal to a .

Given a probability distribution $\mu(x)$ in \mathbb{R}^n and $\alpha \in \mathbb{N}_r^n$, then the moment of $\mu(x)$ at order α is defined as:

$$y_{\alpha} = y_{\alpha_1, \dots, \alpha_n} = \mathbb{E}[x^{\alpha}] = \int x^{\alpha} \mu(x) dx. \quad (3)$$

We construct the (truncated) moment matrix $M_r(y) \in \mathbb{R}^{s(r) \times s(r)}$ via a $s(2r)$ -sequence $y = (y_{\alpha})$, with rows and columns labeled the same as in (1). For example, moment

matrix $M_2(y)$, with $n = 2, r = 2$, is:

$$M_2(y) = \begin{bmatrix} y_{0,0} & y_{1,0} & y_{0,1} & y_{2,0} & y_{1,1} & y_{0,2} \\ y_{1,0} & y_{2,0} & y_{1,1} & y_{3,0} & y_{2,1} & y_{1,2} \\ y_{0,1} & y_{1,1} & y_{0,2} & y_{2,1} & y_{1,2} & y_{0,3} \\ y_{2,0} & y_{3,0} & y_{2,1} & y_{4,0} & y_{3,1} & y_{2,2} \\ y_{1,1} & y_{2,1} & y_{1,2} & y_{3,1} & y_{2,2} & y_{1,3} \\ y_{0,2} & y_{1,2} & y_{0,3} & y_{2,2} & y_{1,3} & y_{0,4} \end{bmatrix} \quad (4)$$

Suppose $y = (y_{\alpha}) \subset \mathbb{R}$ be a sequence indexed by $\alpha \in \mathbb{N}_r^n$, and let the $\mathcal{L}_y : \mathbb{R}[x] \rightarrow \mathbb{R}$ be the linear functional:

$$f(x) = \sum_{\alpha} f_{\alpha} x^{\alpha} \mapsto \mathcal{L}_y(f) = \sum_{\alpha} f_{\alpha} y_{\alpha}. \quad (5)$$

The functional (5) can be interpreted as substituting the monomials x^{α} in $f(x)$ by corresponding y_{α} to obtain the numerical value. Then $M_r(y)$ can be constructed by:

$$M_r(y)(\alpha, \beta) = \mathcal{L}_y(x^{\alpha} x^{\beta}) = y_{\alpha+\beta}, \alpha, \beta \in \mathbb{N}_r^n, \quad (6)$$

or equivalently, by manipulating the entire $v_r(x)v_r(x)^{\top}$:

$$M_r(y) = \mathcal{L}_y(v_r(x)v_r(x)^{\top}). \quad (7)$$

Finally, we also have the localizing matrix for g_i as:

$$M_{r-d_i}(g_i y) = \mathcal{L}_y(g_i v_{r-d_i}(x)v_{r-d_i}(x)^{\top}). \quad (8)$$

One equivalent formulation of (POP) is infinite-dimensional linear programming over the space of probability with support on the feasible set \mathbb{K} [17, 18], where the objective function is a linear combination of the entries of the moment matrix. The detailed formulation of the infinite-dimensional linear programming formulation is presented in Appendix A.

As searching over an infinitely large moment matrix is impossible, we approximate the solution by sequences y_{α} with finite order $|\alpha| = 2\kappa$. Thus, we have the relaxed SDP in the space of moment matrix $M_{\kappa}(y)$ as follows.

Problem 2 (Semidefinite relaxation of POP).

$$\begin{aligned} \rho_{\kappa}^* &:= \inf_{y \in \mathbb{R}^{s(2\kappa)}} \mathcal{L}_y(p) \\ \text{s.t. } &M_{\kappa}(y) \geq 0, \\ &M_{\kappa-d_j}(g_j y) \geq 0, \forall j \in \{1, \dots, m\}. \end{aligned} \quad (\text{SDP})$$

where p and g_j are polynomials.

Because Problem (SDP) gets more constrained as κ increases, we could gradually approximate the globally optimal solution of (POP). This observation leads to the theory of Lasserre’s hierarchy.

Theorem 1 (Lasserre’s Hierarchy [17, 18]). *Let p^* be the optimum of (POP) and the ρ_{κ}^* (resp. y_{κ}^*) be the optimum (resp. optimizer) of (SDP), then:*

- 1) (Monotone lower bound) ρ_{κ}^* is monotonically increasing and $\rho_{\kappa}^* \uparrow p^*$ as $\kappa \rightarrow \infty$.
- 2) (Rank condition) If the moment matrix satisfies:

$$\text{rank}(M_{\kappa}(y_{\kappa}^*)) = \text{rank}(M_{\kappa-d_g}(y_{\kappa}^*)),$$

then $\rho_{\kappa}^* = p^*$. In this case, y^* is a moment sequence that

admits a representing measure on \mathbb{K} .

- 3) (Number of optimizers) If 2) is satisfied, then the number of optimizers equals to $\text{rank}(M_\kappa(y_\kappa^*))$.
- 4) (Finite convergence) If (POP) satisfy some suitable technical condition, under the assumption that Archimedean-ness condition holds for \mathbb{K} , then $\rho_\kappa^* = p^*$ happens at some finite order κ^* [39]. Note that the actual order κ^* is unknown in advance.

Lasserre's hierarchy indicates that one can try from the SDP relaxation with the lowest order and test the rank condition until it is satisfied to obtain the globally optimal solution. For a wide range of applications that only have one optimal solution [44, 51], the rank one optimality condition is expected using Lasserre's hierarchy.

Remark 1 (Rank one optimality condition). *If $\text{rank}(M_\kappa(y_\kappa^*)) = 1$, then $\text{rank}(M_{\kappa-d_g}(y_\kappa^*)) = 1$ as $M_{\kappa-d_g}(y_\kappa^*)$ is a non-zero principle submatrix of $M_\kappa(y_\kappa^*)$.*

B. Rigid body dynamics

We consider special Euclidean group $\text{SE}(3)$ as the configuration space of rigid body motion, where the state $X = \begin{bmatrix} R & p \\ 0 & 1 \end{bmatrix} \in \text{SE}(3)$ can be represented by the orientation

$$R \in \text{SO}(3) = \{R \in \mathbb{R}^{3 \times 3} \mid R^\top R = I_3, \det(R) = 1\},$$

and position $p \in \mathbb{R}^3$. On $\text{SE}(3)$, the twist is defined as the concatenation of linear velocity v and angular velocity ω in the body frame, i.e.,

$$\xi := \begin{bmatrix} \omega \\ v \end{bmatrix} \in \mathbb{R}^6, \xi^\wedge = \begin{bmatrix} \omega^\times & v \\ 0 & 0 \end{bmatrix} \in \mathfrak{se}(3),$$

where $(\cdot)^\times$ satisfies $a^\times b = a \times b$, $a, b \in \mathbb{R}^3$. Note that $\mathfrak{se}(3)$ is the tangent space at the identity $X = I$, and $X\xi^\wedge \in T_X\text{SE}(3)$. The reconstruction equation gives the Equation of Motion (EOM) in continuous time:

$$\dot{X} = X\xi^\wedge. \quad (9)$$

We have the inertia matrix J_b and the kinetic energy:

$$J_b := \begin{bmatrix} I_b & 0 \\ 0 & mI_3 \end{bmatrix}, \quad T(\xi) := \frac{1}{2}\xi^\top J_b \xi, \quad (10)$$

where $I_b \in \mathbb{R}^{3 \times 3}$ is the moment of inertia in the body frame and m is the body mass. We arrive at the Euler-Poincaré equation [52, 53] if we take a variation in $T_X\text{SE}(3)$:

$$J_b \dot{\xi} + \begin{bmatrix} \omega^\times & v^\times \\ 0 & \omega^\times \end{bmatrix} J_b \xi = 0. \quad (11)$$

The challenge of applying Lasserre's hierarchy is to represent the rigid body motion via polynomials. Although one can apply conventional integration schemes such as explicit Euler or Runge-Kutta method on (11) in vector space, the integration of the continuous time EOM (9) on $\text{SE}(3)$ involves the exponential map that does not have polynomial formulations in finite order [54, 55]. If one uses Euler angles to parameterize $R \in \text{SO}(3)$, then a mixture of trigonometric polynomial and

$\mathbb{R}[x]$ is expected, which highly increases the complexity [38]. Instead, we implement the Lie Group Variational Integrator (LGVI) that approximates the generalized velocity via the configuration state to avoid the issue of integrating the continuous time EOM [19].

C. Variational integrator

Consider a mechanical system with the configuration space Q . We denote the configuration state as $q \in Q$ and the generalized velocity as $\dot{q} \in T_q Q$. Then we have the Lagrangian given the kinetic and potential energy $T(\dot{q}), V(q)$:

$$L(q, \dot{q}) := T(\dot{q}) - V(q). \quad (12)$$

The key idea of a variational integrator is to discretize the Lagrangian (12) to obtain the discrete-time EOM [19]. The discretization scheme ensures that the Lagrangian is conserved in the discrete-time, thus having superior energy conservation property in the long duration.

We define the time step $h \in \mathbb{R}$ and the time sequence $\{t_k = kh \mid k = 0, \dots, N\} \subset \mathbb{R}$. Thus the discrete Lagrangian $L_d : Q \times Q \rightarrow \mathbb{R}$ could be considered as the approximation of the action integral via

$$L_d(q_k, q_{k+1}) \approx \int_{t_k}^{t_{k+1}} L(q, \dot{q}) dt. \quad (13)$$

In this work, we consider the midpoint approximation [19]:

$$L_d(q_k, q_{k+1}) = hT\left(\frac{q_{k+1} - q_k}{h}\right) - hV\left(\frac{q_{k+1} + q_k}{2}\right). \quad (14)$$

Then the discrete variant of the action integration becomes:

$$S_d = \sum_{k=0}^{N-1} L_d(q_k, q_{k+1}). \quad (15)$$

Finally, we take variation in TQ and group the term corresponding to $\delta q_k \in T_{q_k} Q$ as the discrete version of integration by parts [19]:

$$\begin{aligned} \delta S_d &= D_1 L_d(q_0, q_1) \cdot \delta q_0 + D_2 L_d(q_{N-1}, q_N) \cdot \delta q_N \\ &+ \sum_{k=1}^{N-1} (D_2 L_d(q_{k-1}, q_k) + D_1 L_d(q_k, q_{k+1})) \cdot \delta q_k. \end{aligned} \quad (16)$$

where D_i denotes the derivative with respect to the i -th argument. By the least action principle, the stationary point can be derived:

$$D_1 L_d(q_k, q_{k+1}) + D_2 L_d(q_{k-1}, q_k) = 0. \quad (17)$$

To incorporate the external force $f \in T_q^* Q$, we can compute the action integral again using the midpoint approximation as:

$$\int_{t_k}^{t_{k+1}} f(t) \cdot \delta q \approx \frac{h}{2} f(t_k) \cdot \delta q_k + \frac{h}{2} f(t_{k+1}) \cdot \delta q_{k+1}, \quad (18)$$

and then incorporate it into (17). We will later show that discretizing Lagrangian on $\text{SE}(3)$ results in polynomial dynamics.

IV. METHOD AND MAIN RESULTS

This section introduces our method to formulate the kinodynamic motion planning problem as exact POP using matrix Lie group formulations.

A. Problem formulation

In what follows, we consider the discrete-time kinodynamic motion planning problem of a rigid body system.

Problem 3 (Discrete Kinodynamic Motion Planning).

$$\begin{aligned} \min_{Y_k, u_k} \quad & \Psi(Y_N) + \sum_{k=0}^{N-1} L(Y_k, u_{k+1}) \\ \text{s.t.} \quad & D(Y_{k+1}, Y_k, u_{k+1}) = 0, \quad k = 0, \dots, N-1, \\ & u_{\min} \leq u_k \leq u_{\max}, \quad H(Y_{k+1}) \geq 0, \quad Y_0 = Y_{\text{init}}. \end{aligned} \quad (19)$$

We require that the system state Y contains the configuration state $X \in \text{SE}(3)$ and velocity $\xi \in \mathfrak{se}(3)$ or its discrete variants. $D(\cdot, \cdot)$ is the EOM subject to the initial condition $Y_0 = Y_{\text{init}}$. For a rigid body system, we consider the discretized motion by (9) and (11). u_{\max} and u_{\min} are the input constraints, and $H(Y) \geq 0$ denotes other constraints, including constraints of $\text{SO}(3)$ manifold and obstacle avoidance. $\Psi(\cdot)$ is the terminal cost, and $L(\cdot, \cdot)$ is the stage cost. If we consider the terminal constraint, we replace $\Psi(\cdot)$ with the equality constraint $Y_N = Y_g$ considering the terminal state Y_g .

To apply Lasserre's hierarchy, we require that all the costs and constraints in Problem 3 are polynomials. As we applied a direct collocation [2, 56] style formulation, the order of polynomial will not grow as the planning horizon increases.

B. Polynomial dynamics constraints

We now derive the dynamics model on $\text{SE}(3)$ via LGVI [57–60]. The derivation for on $\text{SO}(3)$ has been well-established in [57–59]. However, a formulation on $\text{SE}(3)$ suitable for POP implementation is absent. We apply the midpoint approximation (14) to represent the twist ξ_k using the configuration state:

$$F_k := R_k^{-1} R_{k+1} \approx I + h\omega_k^\times, \quad \omega_k^\times \approx \frac{F_k - I}{h}, \quad (20)$$

$$\dot{p}_k = R_k v_k \approx \frac{p_{k+1} - p_k}{h}, \quad v_k \approx \frac{R_k^\top (p_{k+1} - p_k)}{h}, \quad (21)$$

with $F_k \in \text{SO}(3)$ the pose change. We refer to [58] for the expression of the kinetic energy of rotation. Then by (14), the discrete kinetic and potential energy takes the form:

$$\begin{aligned} T_d &:= \frac{1}{2h} \text{tr}((F_k - I)I^b(F_k - I)^\top) + \frac{1}{2h} m \|p_{k+1} - p_k\|^2, \\ V_d &:= hm \frac{p_{k+1} + p_k}{2} \cdot g, \end{aligned} \quad (22)$$

where $g \in \mathbb{R}^3$ is the gravity and I^b the nonstandard moment of inertia [57] that relate the standard moment of inertia I_b by $I_b = \text{tr}(I^b)I_3 - I^b$. Then we define the variation $\delta X \in T_X \text{SE}(3)$ as:

$$\delta X = X \delta \eta^\wedge \in T_X \text{SE}(3), \quad \delta \eta^\wedge = \begin{bmatrix} \delta \omega^\times & \delta \rho \\ 0 & 1 \end{bmatrix} \in \mathfrak{se}(3). \quad (23)$$

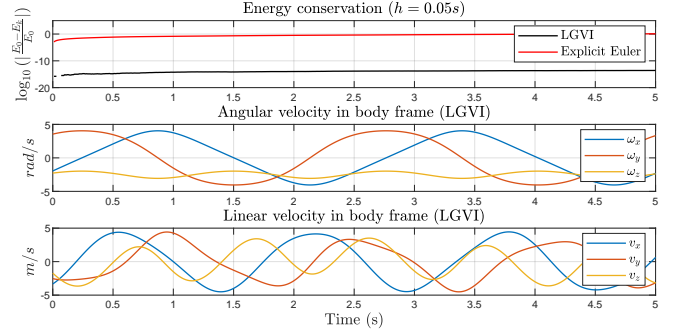


Fig. 2: Comparison of the proposed LGVI with explicit Euler integrator for the rigid body system. The presented twists are computed by LGVI. Considering the energy at time step k , the normalized energy loss $\frac{|E_k - E_0|}{E_0}$ is negligible for LGVI while the explicit Euler integrator soon diverges.

The detailed derivation and the explanation of the I^b are well presented in [57, 58]. Here we only derive the position part not presented in the existing literature. Consider V_d and

$$T_{d,p}(p_k, p_{k+1}) = \frac{1}{2h} m \|p_{k+1} - p_k\|^2,$$

then we have the variation of position in the world frame as $\delta p = R \delta \rho$. Using (17), we have:

$$\begin{aligned} D_1 T_{d,p} &= m \left(\frac{p_k - p_{k+1}}{h} \right) \cdot R_k \delta \rho_k = m (R_k^\top \frac{p_k - p_{k+1}}{h}) \cdot \delta \rho_k \\ D_2 T_{d,p} &= m \left(\frac{p_k - p_{k-1}}{h} \right) \cdot R_k \delta \rho_k = m (R_k^\top \frac{p_k - p_{k-1}}{h}) \cdot \delta \rho_k \end{aligned} \quad (24)$$

Similarly, we have the variation for the potential energy as

$$D_1 V_d = D_2 V_d = \frac{hmg}{2} \cdot R_k \delta \rho_k = R_k^\top \frac{hmg}{2} \cdot \delta \rho_k \quad (25)$$

We wrap up (24) and (25) to obtain

$$m R_k^\top \frac{p_{k+1} - p_k}{h} = m R_k^\top \frac{p_k - p_{k-1}}{h} + R_k^\top mgh. \quad (26)$$

Then, by substituting (20) and (21) into (26), we get

$$m v_{k+1} = m F_k^\top v_k + hm R_{k+1} g. \quad (27)$$

We now present the LGVI for the unconstrained rigid body:

$$\begin{aligned} I^b F_{k+1}^\top - F_{k+1} I^b &= F_k^\top I^b - I^b F_k, \\ m v_{k+1} &= m F_k^\top v_k + hm R_{k+1} g. \end{aligned} \quad (28)$$

We note that all constraints are polynomials with degrees up to two. Similar derivation for $\text{SE}(3)$ has been seen in the research [59, 60]. However, the presented derivation directly applies variations on $T\text{SE}(3)$ in discrete time and does not rely on the continuous angular velocity ω as in [60]. The elimination of ω is more suitable for controller design as it is redundant if we have its discrete variant F_k . The method in [59] does not consider v_k in the tangent space, which is unsuitable for controller design. To verify the correctness of the derived integrator, we plot the kinetic energy and twist for the system without gravity in Fig. 2. We can see that the kinetic energy is conserved in the long run, while the popular explicit Euler method with dynamics (11) diverges fast.

C. Polynomial kinematics constraints

We consider the midpoint approximation as our discrete-time equation of motion for the kinematic part:

$$R_{k+1} = R_k F_k, \quad p_{k+1} = h R_k v_k + p_k, \quad (29)$$

which are also quadratic polynomials. As $R \in \text{SO}(3)$ contains nine entries while $\dim \text{SO}(3) = 3$, we need additional constraints. Consider the column space:

$$R := [r_1, r_2, r_3] \in \mathbb{R}^{3 \times 3}, \quad r_1, r_2, r_3 \in \mathbb{R}^3.$$

$R \in \text{SO}(3)$ is equivalent to the following 15 quadratic equality constraints:

$$\begin{aligned} \|r_1\|^2 - 1 &= \|r_2\|^2 - 1 = \|r_3\|^2 - 1 = 0, \\ r_1^\top r_2 &= r_2^\top r_3 = r_1^\top r_3 = 0, \\ r_1 \times r_2 - r_3 &= r_2 \times r_3 - r_1 = r_3 \times r_1 - r_2 = 0_{3 \times 1}. \end{aligned} \quad (30)$$

The first six equations ensure that r_i are orthonormal to each other, and the last nine equations ensure r_i follows the right-hand rule, which is equivalent to the determinant constraints but is quadratic.

We introduce two variables, c and s that satisfy $c^2 + s^2 = 1$ to indicate rotation about a single axis:

$$R_x = \begin{bmatrix} 1 & 0 & 0 \\ 0 & c & -s \\ 0 & s & c \end{bmatrix}, R_y = \begin{bmatrix} c & 0 & s \\ 0 & 1 & 0 \\ -s & 0 & c \end{bmatrix}, R_z = \begin{bmatrix} c & -s & 0 \\ s & c & 0 \\ 0 & 0 & 1 \end{bmatrix}. \quad (31)$$

$R_i(\theta)$ denotes a rotation of θ angle about axis i .

D. Sparsity pattern

As Problem 3 satisfies the Markov assumption, we show it enables the use of Correlative Sparsity (CS) that greatly reduces the computational burden [41]. Consider the full dynamics model represented in (28) and (29), we can formulate Y in Problem 3 as $Y_k := (R_k, p_k, F_k, v_k)$. Then we also include (28)-(30) in constraints D and H . We partition the state into N sets $y(I_k) = \{(Y_i, Y_{i-1}, u_i) | i \in I_k\}$ indexed by $I_k = \{k, k+1\}, k = 1, 2, \dots, N$. Then we can verify the running intersection property [41]:

$$\forall k = 1, \dots, q-1, \exists s \leq k, I_{k+1} \cap (\cup_{j=1}^k I_j) \subseteq I_s,$$

by selecting $s = k$, i.e. $I_{k+1} \cap (\cup_{j=1}^k I_j) = \{k+1, k+2\} \cap (\cup_{j=1}^k I_j) = \{k+1\} \in I_k$. We can see that the cost and dynamic constraints can also be partitioned into such indexed sets as $D(Y_{k+1}, Y_k, u_{k+1}) = 0$, $H(Y_{k+1}) = 0$ and $L(Y_k, u_k)$ only involves variable $y(I_k)$. These properties enable the sparse moment relaxation to have the same result as the dense version if one breaks the dense matrix $M_\kappa(y)$ to N smaller ones that only involve variables in $y(I_k)$ [41]. The detail of CS is presented in Appendix B. When the relaxation order is determined, we can see that the size of the variable grows linearly with respect to the planning horizon [18, 41].

Other than CS, Term Sparsity (TS) has also been exploited to reduce the computational burden further [40, 44] by eliminating more variables in the moment matrix. Though

relaxation with TS is looser than CS, the computation time is greatly reduced.

V. NUMERICAL SIMULATIONS

In this section, we apply the proposed framework to various robotics applications.

A. Simulation setup

1) *Relaxation scheme*: For all tasks, the dynamics, constraints, and objective functions are quadratic polynomial functions; thus, we have the lowest order for Lasserre's hierarchy $\kappa = 1$ and the degree parameter $d_g = 1$. However, $\kappa = 1$ only returns a trivial lower bound with infeasible solutions. Thus we try $\kappa = 2$ and find it works well for our cases.

We use the recent state-of-the-art tool CS-TSSOS [40, 43, 61, 62] to explore the CS and TS pattern. Chordal extension [61] is applied to boost both CS and TS by either extending matrix size (for CS) or reducing more terms (for TS). As the CS does not sacrifice the tightness and the problem size is huge, we always exploit the CS pattern. The CS-TSSOS supports the maximal or approximately smallest chordal extension, which is denoted as MD and block, respectively, referring to the programming API. Assume that the global optimum of (POP) is p^* and the optimum of the (SDP) or local Nonlinear Programming (NLP) solver is ρ , then we have the following inequalities:

$$\begin{aligned} \rho_{TS+MD} &\leq \rho_{TS+block} \leq \rho_{CS} \leq \rho_{CS+MD} \\ &\leq \rho_{dense} \leq p^* \leq \rho_{NLP}, \end{aligned} \quad (32)$$

where the subscripts denote different sparsity patterns at the same order κ . As the NLP solver are based on local gradient information, only local optimum is guaranteed. Therefore, ρ_{NLP} serves as an upper bound of p^* .

2) *Evaluation metric*: As the optimal value of (POP) can not be greater than ρ_{NLP} , then the problem is upper and lower bounded by the SDP and NLP result. Thus, we can use the relative suboptimality as an index of the relaxation gap:

$$\epsilon := \frac{\rho_{NLP} - \rho_{SDP}}{\rho_{NLP}}. \quad (\text{suboptimality})$$

As the rank condition is subject to numerical error, we instead check the eigenvalues of each sub-moment matrix as is shown in Remark 2 in Appendix B. We check if each moment matrix is rank-one, assuming the unique minimizer. Assume the eigenvalues of k -th moment matrix $\lambda_{k,i}$ are ranked by their $|\lambda_{k,i}|$ in descending order. Then we compute the ratio between the first and the second one to represent the rank condition:

$$\delta_k = \frac{|\lambda_{k,2}|}{|\lambda_{k,1}|} \leq 1, \delta = \max_k \delta_k. \quad (\text{rank condition})$$

As the numerical accuracy is still the bottleneck of the current SDP solvers for problems of this size, δ will only be used for comparison with ϵ .

3) *Software and hardware setup*: The CS-TSSOS is implemented in Julia's open-source package [40, 43]. CS-TSSOS converts (SDP) to its dual and passes to the solver MOSEK

[63]. As MOSEK is based on the primal-dual interior point method, thus it can generate a certificate for infeasibility [64]. We use the certificate returned by MOSEK to indicate the feasibility of the SDP. If (SDP) is infeasible, then its dual will be unbounded [34, 63]. Thus MOSEK will return large objective values even if it fails to generate the infeasibility certificate. MOSEK also returns `SLOW_PROGRESS` flag if the problem does not converge successfully, possibly around a minimum. As the SDP relaxation of POP does not ensure feasibility or local optimality if the SDP is not tight [18], for the drone landing case, we use the general purpose NLP solver IPOPT [65] for local search and the solution from SDP as the initial guess. All experiments are launched on a desktop equipped with Intel i9-11900KF CPU and 128 GB memory.

B. Inverse kinematics for serial manipulator

We consider the inverse kinematics problem for n Degrees of Freedom (DOF) serial manipulator with revolute joints. We use $X_k \in \text{SE}(3)$ to represent the pose of k -th joint. Each joint is modeled as rotating about the local z -axis, i.e., R_z described in (31) with the angle denoted by c_k and s_k . Note that one can also use DH parameters with similar results. Thus, we have the kinematics chain:

$$X_{k+1} = X_k A_{k+1} T_k, \quad X_0 = I, \quad (33)$$

with

$$T_k := \begin{bmatrix} R_k^c & 0 \\ 0 & 1 \end{bmatrix}, A_k := \begin{bmatrix} R_k^z & R_k^z p_k^c \\ 0 & 1 \end{bmatrix}. \quad (34)$$

In this formulation, p_k^c is the constant vector defining the arm, and A_k is the action that describes the rotation of the arm about the z -axis of joint X_k . T_k is a constant that re-orientates the pose for joint X_{k+1} . For joint angle constraints $\theta_{\min} \leq \theta \leq \theta_{\max}$, we have the following inequality:

$$\cos\left(\theta - \frac{\theta_{\max} + \theta_{\min}}{2}\right) \geq \cos \frac{\theta_{\max} - \theta_{\min}}{2}. \quad (35)$$

Then the IK problem for an N DOF serial manipulator to reach the target pose $T_g \in \text{SE}(3)$ is formulated as follows.

Problem 4 (IK for N-DOF serial manipulator).

$$\begin{aligned} \min_{\{c_k, s_k, X_k\}} & \sum_{k=1}^N (c_k - c_k^r)^2 + (s_k - s_k^r)^2 \\ \text{s.t.} & X_{k+1} = X_k A_{k+1} T_k, \quad k = 0, 1, \dots, N-1. \\ & X_k \in \text{SE}(3), \quad c_{k+1}^2 + s_{k+1}^2 = 1, \\ & c_{k+1} \bar{c}_{k+1} + s_{k+1} \bar{s}_{k+1} \geq c_{\text{lim}}, \\ & X_0 = I, X_N = X_g. \end{aligned} \quad (36)$$

Where \bar{c}_k, \bar{s}_k and c_{lim} correspond to terms in the expansion of (35). The cost function is parameterized by a reference joint angle $c_k^r = 1$ and $s_k^r = 0$ in our case to ensure unique solutions. We tested the proposed algorithm on the 6-DOF manipulator PUMA 560 that has analytical IK solutions [66]. As is shown in Fig. 3, we uniformly sample 14553 positions in the workspace with random rotations. We validate the algorithm based on the quality of infeasibility detection, and

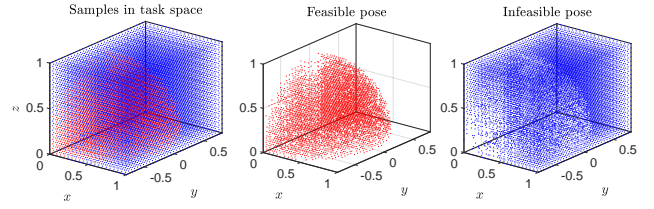


Fig. 3: Samples in the workspace for 6-DOF PUMA 560 manipulator. We sampled $21 \times 21 \times 33 = 14553$ points with 5 cm intervals in the workspace of size $1m \times 1m \times 1.6m$. The 4712 feasible poses are denoted as red, while the 9841 infeasible poses are denoted as blue.

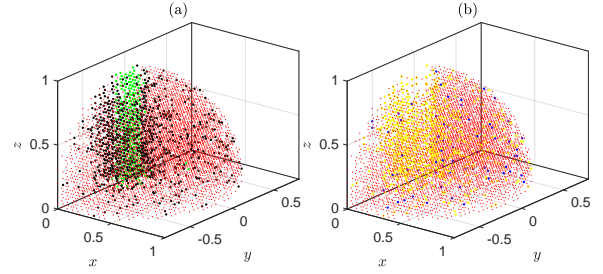


Fig. 4: IK solution for 6-DOF PUMA 560 manipulator. (a) applied the CS at $\kappa = 2$, the green dots denote the infeasible pose that the solver does not generate an infeasibility certificate, and the objective value is smaller than the threshold. The black dots denote the feasible poses that the solver does not converge and terminates as `SLOW_PROGRESS`. (b) applied CS+MD at $\kappa = 2$ with chordal extension. All the green dots in (a) can be certified as infeasible using this relaxation scheme via the certificate or unreasonably large dual problem values. The yellow dots denote the feasible poses with convergent SDP solution. The blue dots denote the case that is still not convergent at this relaxation scheme. When moving to $\kappa = 3$, only one of the cases converges.

all the seven joint poses X_k (including the base joint) directly recovered from SDP without refining. We consider the pose as infeasible if MOSEK returns an infeasibility certificate or unreasonably large objective value. We set the threshold as 1000, which is sufficiently larger than the maximal possible objective of Problem 4.

The main results are summarized in Table I and illustrated in Fig. 4. We first apply CS at $\kappa = 2$. As shown in Fig. 4(a), we can see that 239 poses are infeasible but detected as feasible. We also have 879 feasible poses that the solver fails to converge and terminates as `SLOW_PROGRESS`. Then we apply a slightly tighter relaxation, i.e., CS+MD at $\kappa = 2$, to improve the result. As is in Fig. 4(b), all the infeasible points can be certified, and 812 out of the 879 feasible cases converge. For the other 67 cases, we move to $\kappa = 3$ with CS, but only 1 of them converges. Tighter relaxation, such as CS+MD at $\kappa = 3$, will use up the memory.

For the cases successfully solved by MOSEK, the average rotation and position errors are negligible. For the failed cases that terminated as `SLOW_PROGRESS`, some cases have errors at a comparable level while some have position errors that can reach 1 m. Compared to the mix-integer programming-based method [13], the proposed algorithm has highly accurate solutions when the SDP converges to the optimum, as the kinematic model we use is exact. As [13] can not avoid the

TABLE I: The average performance of SDP relaxation on Puma 560 manipulator. We launch all the tests from a looser relaxation scheme and move to a tighter scheme for failed cases. The runtime is based on each individual relaxation scheme, while the other indices are accumulated from the lowest scheme. The pose error is based on cases successfully solved by MOSEK.

Relaxation order (κ)	2	2	3
Sparsity pattern	CS	CS+MD	CS
Average solution time (s)	7.8	918.7	804.8
Maximum solution time (s)	18.5	2117.9	1886.5
Average joint orientation error (deg)	$6.93e^{-5}$	$6.93e^{-5}$	$6.93e^{-5}$
Maximal joint orientation error (deg)	0.0231	0.0231	0.0231
Average joint position error (cm)	$1.45e^{-5}$	$1.45e^{-5}$	$1.45e^{-5}$
Maximal joint position error (cm)	0.0191	0.0191	0.0191
Percentage of infeasibility detection	97.57%	100.0%	100.0%
Percentage of convergent SDP (feasible poses)	81.35%	98.58%	98.60%
Overall successful rate (all poses)	92.32%	99.54%	99.55%

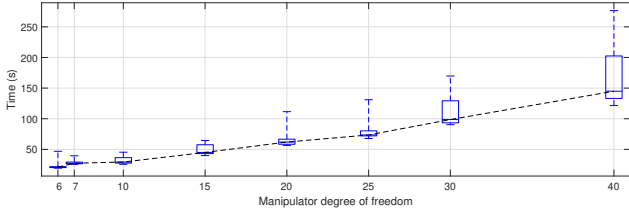


Fig. 5: The runtime for the IK problem with DOF ranging from 6 to 40 tested on 50 randomly generated manipulators. We find that the time complexity is linear with respect to the DOF if CS is applied. The median value is denoted as connected by the black line.

inaccuracy due to the partition of $SO(3)$ manifold, the position error can be centimeters. Both our method and [16] are based on moment relaxation and suffer from similar numerical issues when solving the SDP, while the overall success rates are at the same level.

Problem 4 has the same sparsity pattern as the kinodynamic planning Problem 3. Thus, we further tested the runtime for Problem 4 with DOF ranging from 6 to 40 with 50 randomly generated parameters R_k^c and p_k^c with CS at $\kappa = 2$ to evaluate the complexity of the algorithm. As is shown in Fig. 5, the runtime grows linearly with respect to the DOF, which is consistent with the complexity analysis presented in [41]. In comparison, [13] has exponential computation time with respect to the planning horizon due to the combinatorial formulation. As [16] is a dense formulation, the number of variables and degrees grows simultaneously. Considering the size of the moment matrix, [16] has at least polynomial complexity with respect to the length of the kinematic chain.

C. 3D drone landing

In this task, we consider landing a drone from an initial pose while avoiding obstacles. We assume that the drone is controlled by torque $\tau \in \mathbb{R}^3$ and total thrust force $f^z \in \mathbb{R}$

TABLE II: Drone landing parameters

Simulation constants	Values	Control parameters	Values.
Mass - m	0.5 (kg)	P	[100, 10, 100, 100]
Inertial - I_b	diag(0.3, 0.2, 0.3) (kg/m ²)	Q	[0.1, 10, 0.1, 1]
Gravity - g	[0, 0, -9.81] ^T (m/s ²)	U	[0.1, 0.1]
Time step - h	0.1667s / 0.125s	$[\tau_{\min}^x, \tau_{\max}^x]$	[-5, 5]
Planning horizon - N	30 / 40	$[f_{\min}^z, f_{\max}^z]$	[- ∞ , ∞]
Obstacle 1	$x^2 + (y - 0.5)^2 \geq 0.25$	p_0, v_0, I_0	[1, 1, 3] ^T , $0_{3 \times 1}$, I_3
Obstacle 2	$(x - 0.6)^2 + (y - 0.5)^2 \geq 0.25$	$R_0 = R_y(\theta)$	$\theta = 0^\circ, 60^\circ, 90^\circ, 120^\circ, 180^\circ$
Height constraints	$z \geq 0$		

along the z -axis, both in the body frame. Thus we have the kinematics model (29) and the forced drone dynamics:

$$\begin{aligned} I^b F_{k+1}^\top - F_{k+1} I^b &= F_k^\top I^b - I^b F_k + h^2 \tau_{k+1}^\times, \\ m v_{k+1} &= m F_k^\top v_k + h(B f_{k+1}^z + m R_{k+1} g), \end{aligned} \quad (37)$$

with $B = [0, 0, 1]^\top$. We then define the quadratic cost:

$$\begin{aligned} \Phi(Y_N) &= P_1 \|R_N - I\|_{F,I}^2 + P_2 \|F_N - I\|_{F,I}^2 \\ &\quad + P_3 \|p_N\|^2 + P_4 \|v_N\|^2, \end{aligned} \quad (38)$$

$$\begin{aligned} L(Y_k, u_{k+1}) &= Q_1 \|R_k - I\|_{F,I}^2 + Q_2 \|F_k - I\|_{F,I}^2 \\ &\quad + Q_3 \|p_k\|^2 + Q_4 \|v_k\|^2 + U_1 \|\tau_{k+1}\|^2 + U_2 \|f_{k+1}^z\|^2, \end{aligned} \quad (39)$$

where $\|X\|_{F,P} = \sqrt{\text{tr}(X^\top P X)}$, $P \geq 0$, is the weighted Frobenius norm. The system parameters and cost functions are shown in Table. II. We set the drone at an initial position with different pitch angles. We launch the trajectory optimization with one of the obstacles or in free space. Obstacle 2 blocks more waypoints of the trajectory planning in the free space compared to obstacle 1. The whole planning horizon is 5 seconds with 40 steps. For the CS cases without TS, the SDP has too many variables that used up the memory, so we reduced the step number to 30. We start with TS+MD and continue to TS+block or CS if ϵ is large for a former relaxation scheme. Empirically, we find that $\epsilon \leq 1e^{-3}$ results in tight moment relaxation that also guarantees the feasibility of the solution. Thus, we set $\epsilon \leq 1e^{-3}$ as a threshold to decide whether to continue to a tighter relaxation scheme.

The planned trajectories of all cases after being refined by IPOPT are illustrated in Fig. 6, 7 and 8. The statistics of the planned trajectories are presented in Table III, IV, and V. For all tests, TS+MD does not provide an optimality gap smaller than 0.01. For simple cases in free space or with obstacle 1, TS+block can solve all the cases with $\theta \leq 90^\circ$. For $\theta = 120^\circ$, moving to CS also generates certifiable optimality values. While for $\theta = 180^\circ$, the CS does not provide certifiable optimal values. For hard cases with obstacle 2, more numerical issues are presented. Even the CS sparsity pattern does not provide certifiable solutions for $\theta = 60^\circ$ and $\theta = 180^\circ$.

As the solver returned SLOW_PROGRESS for these failed cases, we do not know if the SDP relaxation itself is tight at this order for these initial conditions. However, the solution is still a good initial guess for local search by IPOPT. We can also find that the magnitude of ϵ and δ are closely correlated to each other. When $\epsilon \leq 1e^{-4}$, the rank-one condition will likely satisfy as δ is also small.

We further compare the proposed methods with local solvers. We compute POP using IPOPT and initializations with different qualities. As the moment relaxation already gives an initial guess with guaranteed lower bound by suboptimality metric ϵ , we perturb the refined solution with the smallest ϵ as our initial guess. For the orientation R_k and pose change F_k , we perturb it by rotating with a random angle as $\tilde{R}_k = R_k \exp(\zeta)$ where $\zeta \sim N(0_{3,1}, \Delta^2 I_3)$ is white Gaussian noise. We perform element-wise random perturbation for other variables, such as $\tilde{v}_k = v_k + \zeta$. Then we assign different Δ to

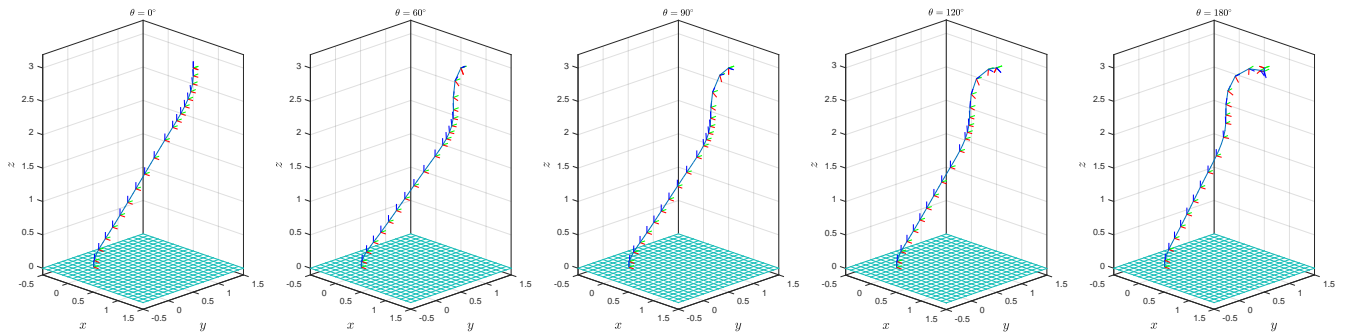


Fig. 6: 3D drone landing task in free space. The drone starts at an initial position $x = 1, y = 1, z = 3$ with zero twists and different initial pitch angles. The robot is guided to land at the origin. The blue, red, and green axes indicate the $z, x,$ and y axes in the body frame. For a large initial pitch angle, the drone adjusts the orientation in the first few steps and then starts to move to the origin. Only part of the waypoints in the tail of trajectories are presented to avoid overlap. The statistics of these cases are presented in Table III.

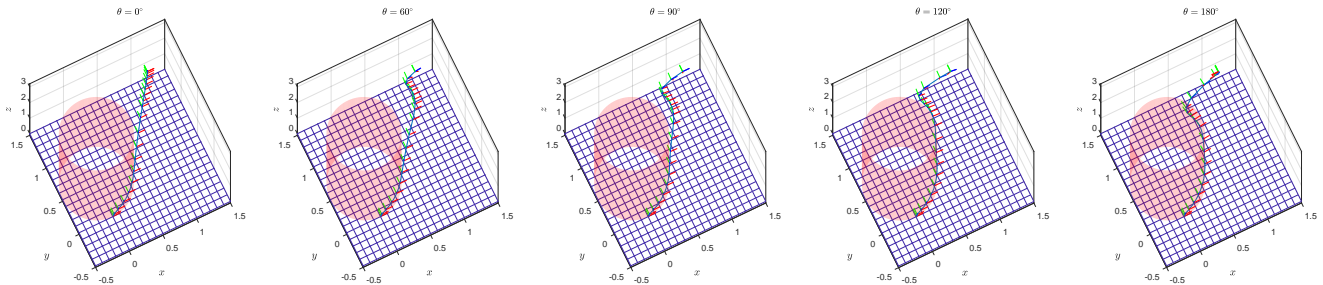


Fig. 7: 3D drone landing task with obstacle 1. Obstacle 1 blocks some of the waypoints computed from the free space task. All these plots converge to a locally feasible path after being refined by IPOPT, and the first 4 cases are certified as globally optimal solutions by metric ϵ . The statistics of these cases are presented in Table IV.

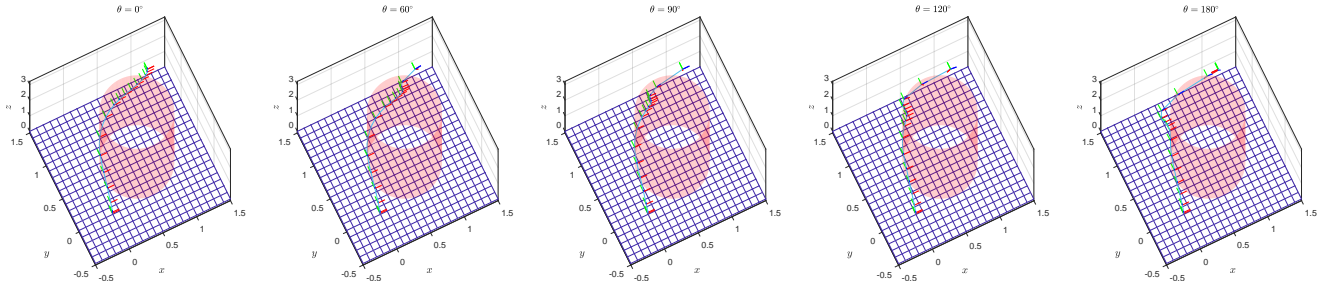


Fig. 8: 3D drone landing task with obstacle 2. Obstacle 2 blocks more waypoints in the free space task than obstacle 1, which makes the SDP harder to converge. All these cases converge to locally feasible solutions after being refined by IPOPT, and the first 4 cases have very small optimality gaps. The statistics of these cases are presented in Table V.

represent the quality of the initial guess. We mainly evaluate the IPOPT solution via the optimality gap ϵ compared to the best-known refined solutions by SDP and the convergent status of IPOPT. For each Δ , we sample 10 times for all the 5 initial conditions and tasks. The result is presented in Table VI. The local solver highly relies on the initial guess quality, as shown in Table VI. However, such a good initial guess is not always available in practice. Though the local search method is fast, it is possible that the solver converges to infeasible points.

VI. DISCUSSIONS

We have shown that Lasserre's hierarchy at the second order can provide rank-one globally optimal solutions for most testing cases of the two case studies. More than 99.5%

of the IK problems can be solved, while the remaining cases are subject to numerical issues. By LGVI, the drone dynamics can be formulated as exact quadratic polynomials, which is not possible using a conventional integration scheme or approximations. The SDP converges well for easy cases with certified globally optimal solutions while suffering from numerical issues for hard cases. From the point of view of computational complexity, the worst-case for arbitrary obstacle configuration still results in SDPs of computationally intractable size. Thus, a convex representation of free space [15], obstacles [30, 67, 68], or risk-bounded contours of [69–71] should be explored.

A more intriguing future direction is to find conditions when such Lie group-based motion planning problems can be tightly

TABLE III: Statistics of drone landing in free space. TS+block can solve all of the cases with pitch angles smaller than 120° . For the harder cases, CS is needed to induce tighter relaxation. These cases are illustrated in Fig. 6.

$R_{y,0}$	0°			60°			90°			120°			180°		
Sparsity	TS+MD	TS+block	CS	TS+MD	TS+block	CS	TS+MD	TS+block	CS	TS+MD	TS+block	CS	TS+MD	TS+block	CS
Suboptimality ϵ	0.0101	$\leq 1e^{-4}$	N/A	0.0235	$\leq 1e^{-4}$	N/A	0.0589	$\leq 1e^{-4}$	N/A	0.3767	0.0046	$\leq 1e^{-4}$	0.4102	0.2054	0.0136
Rank condition δ	0.0968	$\leq 1e^{-4}$	N/A	0.1702	$\leq 1e^{-4}$	N/A	0.4918	$6.302e^{-4}$	N/A	0.8301	0.5824	$\leq 1e^{-4}$	0.9049	0.9653	0.6504
Runtime (s)	397.1	2299.6	N/A	431.4	2185.9	N/A	381.3	2298.5	N/A	373.6	2868.3	6662.0	346.7	3646.5	6820.4

TABLE IV: Statistics of drone landing with obstacle 1. All cases can be tightly solved except the last one. These cases are illustrated in Fig. 7.

$R_{y,0}$	0°			60°			90°			120°			180°		
Sparsity	TS+MD	TS+block	CS	TS+MD	TS+block	CS	TS+MD	TS+block	CS	TS+MD	TS+block	CS	TS+MD	TS+block	CS
Suboptimality ϵ	0.0130	$\leq 1e^{-4}$	N/A	0.0252	$\leq 1e^{-4}$	N/A	0.0608	$\leq 1e^{-4}$	N/A	0.3772	0.0070	$\leq 1e^{-4}$	0.3810	0.2083	0.0205
Rank condition δ	0.0965	$\leq 1e^{-4}$	N/A	0.1696	$\leq 1e^{-4}$	N/A	0.4805	$4.631e^{-4}$	N/A	0.8240	0.5687	$\leq 1e^{-4}$	0.9194	0.9661	0.7051
Runtime (s)	424.0	2598.5	N/A	361.6	2549.9	N/A	426.7	3246.1	N/A	433.5	2863.2	7039.4	409.2	3834.5	8641.7

TABLE V: Statistics of drone landing with obstacle 2. Due to the configurations of the obstacle, this task is more challenging, but the overall optimality gap using CS is small except for the 180° case. These cases are illustrated in Fig. 8.

$R_{y,0}$	0°			60°			90°			120°			180°		
Sparsity	TS+MD	TS+block	CS	TS+MD	TS+block	CS	TS+MD	TS+block	CS	TS+MD	TS+block	CS	TS+MD	TS+block	CS
Suboptimality ϵ	0.0499	0.0275	$7.731e^{-4}$	0.0580	0.0307	0.0035	0.0802	0.0473	$\leq 1e^{-4}$	0.3846	0.0154	$\leq 1e^{-4}$	0.4231	0.2127	0.0167
Rank condition δ	0.1013	0.0738	0.0369	0.1776	0.0661	0.1207	0.5019	0.1849	0.0016	0.8348	0.6049	$\leq 1e^{-4}$	0.9088	0.9632	0.6712
Runtime (s)	391.1	3295.4	8314.3	360.5	3111.7	9310.6	424.2	3471.0	7241.5	416.2	3350.2	7700.8	429.1	3686.7	8180.6

TABLE VI: Statistics of drone landing task solved by IPOPT. We perturb the best optimality guaranteed SDP solution with different noise levels to obtain the initial guess. The average suboptimality is evaluated on each task with 5 initial pitch angles. For each test case, we sample the initial error 10 times. Thus the average suboptimality is evaluated by feasible solutions among the 50 random samples. We show that with a small noise level, IPOPT converges to the best solution obtained by SDP. However, as the noise level increases, the optimality gap grows significantly, and even local feasibility is not guaranteed. We set the computational budget as $1e4$ iterations.

Initialization noise Δ	0.001			0.01			0.1			0.5			1		
Task	Free	Obs-1	Obs-2	Free	Obs-1	Obs-2	Free	Obs-1	Obs-2	Free	Obs-1	Obs-2	Free	Obs-1	Obs-2
Average Suboptimality ϵ	$\leq 1e^{-4}$	0.0115	0.0134	$\leq 1e^{-4}$	0.3644	0.4757	0.2406	0.7727	0.7543	0.5652					
Timeout (out of 50)	0	0	0	0	0	0	0	0	0	12	8	2	25	15	6
Infeasibility (out of 50)	0	0	0	0	0	0	0	0	0	13	11	13	16	23	13

solved via Lasserre’s hierarchy at the second order, despite the numerical challenges. Such efforts would be essential for convex kinodynamic motion planning using the full dynamics model. The LGVI-based formulation can be extended to multi-body systems when additional constraints and multipliers are added [72]. Nonholonomic systems can also be modeled by LGVI, while the discretization of nonholonomic constraints needs more attention [73, 74]. More generally, LGVI is aligned with symmetry-preserving methods in robotics [75] and its applications in various robot perception and control problems from a promising research direction.

The memory and time cost of the proposed algorithm is still high for real-time applications. In view of global optimization, the complexity is linear w.r.t the planning horizon and polynomial order w.r.t the system dimension (consider the size of the moment matrix) when the relaxation order is determined. Such property is an improvement compared to other global optimization methods, such as combinatorial optimization with exponential complexity. To improve the scalability for real-time deployment, combining the global convergence property of SDP [76] and fast local search on Lie groups [77–81], should be considered in the future.

VII. CONCLUSIONS

In this paper, we present the novel result: by formulating the robot dynamics model on Lie groups, one can convert the motion planning problem to polynomial optimization problems that can be solved via Lasserre’s hierarchy. We show that

the proposed formulation converts rigid body dynamics as exact quadratic polynomials. We further formulate the motion planning problem as a sparse moment relaxation problem. Attributed to the low-order and sparse formulation, the resulting SDP has linear complexity with respect to the planning horizon and is computationally tractable for the current solvers. The case study on the inverse kinematics for serial manipulators and 3D drone landing problems suggests that the proposed formulation can successfully provide certified globally optimal solutions for most cases.

APPENDIX A

POP AS INFINITE-DIMENSIONAL LINEAR PROGRAMMING

Problem POP can be converted to the following infinite dimensional linear programming problem over the space of measure [17, 18]:

Problem 5 (Infinite dimension linear programming).

$$p^* := \inf_{\mu \in \mathcal{M}^+(\mathbb{K})} \int_{\mathbb{K}} p(x) d\mu, \quad (\text{LP})$$

with \mathbb{K} the feasible set defined in (POP), $\mathcal{M}(\mathbb{K})$ the set of vector space of finite signed Borel measure and $\mathcal{M}^+(\mathbb{K})$ the convex cone of nonnegative finite Borel measure on \mathbb{K} .

Then, the optimization problem (POP) is equivalent to finding the Dirac measure δ_{x^*} that is associated with the minimizer x^* of (POP). Recall that the Dirac measure has

the property $\int_{\mathbb{K}} p(x) d\delta_{\bar{x}} = p(\bar{x})$, that enables one to select the value of $p(x)$ at a given point \bar{x} .

APPENDIX B

SPARSE MOMENT RELAXATION OF POP

Though Lasserre’s Hierarchy enables one to approximate (POP) by (SDP), the size of (SDP) increases dramatically as κ and n increase. Therefore, one should fully explore the structure of the problem to reduce the computational burden. For many applications in control and planning satisfying the Markov assumption, only states at consecutive time steps appear in the system dynamics. The cost function is usually the sum of stage costs that only contain states within one step. Motivated by this observation, we introduce the correlative sparsity.

We define the index set $I_0 = \{1, \dots, n\}$ be the union of $\cup_{k=1}^q I_k$ of q subsets $I_k \subset I_0$ that partition the variable x . For arbitrary $I_k \subseteq I_0$, let $\mathbb{R}[x(I_k)]$ denote the ring of polynomials in the variable $x(I_k) \in \{x_i | i \in I_k\}$. We also define the index set $J = \{1, \dots, m\}$ that is partitioned in to q different disjoint sets $J_k, k = 1, \dots, q$ to group the constraints $g_j, j = 1, \dots, m$.

Assumption 1 (Sparse structure of (POP), [18, 41]).

- 1) For feasible set \mathbb{K} , there is a large number M , such that $\|x\|_{\infty} \leq M$ for $\forall x \in \mathbb{K}$.
- 2) For every $j \in J_k, g_j \in \mathbb{R}[x(I_k)]$, such that each constraint $g_j(x) \geq 0$ only involves variables in the set $x(I_k) = \{x_i | i \in I_k\}$.
- 3) The objective function $p(x) \in \mathbb{R}[x]$ can be written as $p(x) = \sum_{k=1}^q f_k$, with $f_k \in \mathbb{R}[x(I_k)], k = 1, \dots, q$.
- 4) The index set I_k satisfy the running intersection property:

$$\forall k = 1, \dots, q - 1, \exists s \leq k, I_{k+1} \cap (\cup_{j=1}^k I_j) \subseteq I_s.$$

If (POP) satisfies the assumptions, the following sparse moment relaxations can dramatically reduce the problem size.

Problem 6 (Sparse moment relaxation [18, 41]).

$$\begin{aligned} \rho_{\kappa}^* &:= \inf_{y \in \mathbb{R}^{s(2\kappa)}} \mathcal{L}_y(p) \\ \text{s.t. } & M_{\kappa}(y, I_k) \geq 0, \\ & M_{\kappa-d_g}(g_j y, I_k) \geq 0, \\ & j \in J_k, k = 1, \dots, q. \end{aligned} \quad (\text{sparse-SDP})$$

Where $M_{\kappa}(y, I_k)$ denotes the moment matrix formed by the variables that appear in the set I_k . We also have a slightly different rank condition and the special rank-one case for the sparse moment relaxation.

Theorem 2 (Rank condition for (sparse-SDP) [18, 41]). (sparse-SDP) is tight, if:

- 1) If Assumption 1 is satisfied for (POP), and,
- 2) $\text{rank}(M_{\kappa}(y_{\kappa}^*, I_k)) = \text{rank}(M_{\kappa-d_g}(y_{\kappa}^*, I_k)), k = 1, \dots, p$, and,
- 3) $\text{rank}(M_{\kappa}(y_{\kappa}^*, I_{jk})) = 1$ for all pairs (i, k) with $I_{jk} := I_j \cap I_k \neq \emptyset$.

Remark 2 (Rank one optimality condition for (sparse-SDP)). For the special case of rank one condition, we will only need to check the first two conditions in Theorem 2 as any $M_{\kappa}(y, I_{jk})$ can become a principle submatrix of the $M_{\kappa}(y, I_k)$ or $M_{\kappa}(y, I_j)$ after proper invertible row and column permutations. Thus, $M_{\kappa}(y, I_{jk})$ is rank one if $M_{\kappa}(y, I_k)$ or $M_{\kappa}(y, I_j)$ are rank one matrix.

REFERENCES

- [1] Bruce Donald, Patrick Xavier, John Canny, and John Reif. Kinodynamic motion planning. *Journal of the ACM (JACM)*, 40(5):1048–1066, 1993. 1
- [2] John T Betts. Survey of numerical methods for trajectory optimization. *Journal of guidance, control, and dynamics*, 21(2):193–207, 1998. 1, 5
- [3] Behçet Açıkmeşe, John M Carson, and Lars Blackmore. Lossless convexification of nonconvex control bound and pointing constraints of the soft landing optimal control problem. *IEEE Transactions on Control Systems Technology*, 21(6):2104–2113, 2013. 1
- [4] John H Reif. Complexity of the mover’s problem and generalizations. In *Annual Symposium on Foundations of Computer Science*, pages 421–427. IEEE Computer Society, 1979. 1
- [5] John E Hopcroft, Jacob Theodore Schwartz, and Micha Sharir. On the complexity of motion planning for multiple independent objects; PSPACE-hardness of the “warehouseman’s problem”. *International Journal of Robotics Research*, 3(4):76–88, 1984.
- [6] John Canny. A new algebraic method for robot motion planning and real geometry. In *Annual Symposium on Foundations of Computer Science*, pages 39–48. IEEE, 1987. 1
- [7] Arthur Richards and Jonathan P How. Aircraft trajectory planning with collision avoidance using mixed integer linear programming. In *Proceedings of the American Control Conference*, volume 3, pages 1936–1941. IEEE, 2002. 1, 2
- [8] Tom Schouwenaars, Bart De Moor, Eric Feron, and Jonathan How. Mixed integer programming for multi-vehicle path planning. pages 2603–2608. IEEE, 2001. 2
- [9] Robin Deits and Russ Tedrake. Efficient mixed-integer planning for UAVs in cluttered environments. In *Proceedings of the IEEE International Conference on Robotics and Automation*, pages 42–49. IEEE, 2015. 2
- [10] Yanran Ding, Chuazheng Li, and Hae-Won Park. Kinodynamic motion planning for multi-legged robot jumping via mixed-integer convex program. In *Proceedings of the IEEE/RSJ International Conference on Intelligent Robots and Systems*, pages 3998–4005. IEEE, 2020. 2
- [11] Yanran Ding, Chuazheng Li, and Hae-Won Park. Single leg dynamic motion planning with mixed-integer convex optimization. In *Proceedings of the IEEE/RSJ International Conference on Intelligent Robots and Systems*, pages 1–6. IEEE, 2018.
- [12] Robin Deits and Russ Tedrake. Footstep planning on uneven terrain with mixed-integer convex optimization. In *IEEE-RAS international conference on humanoid robots*, pages 279–286. IEEE, 2014. 2
- [13] Hongkai Dai, Gregory Izatt, and Russ Tedrake. Global inverse kinematics via mixed-integer convex optimization. *International Journal of Robotics Research*, 38(12-13):1420–1441, 2019. 1, 2, 7, 8
- [14] Bachir El Khadir, Jean Bernard Lasserre, and Vikas Sindhvani. Piecewise-linear motion planning amidst static, moving, or morphing obstacles. In *Proceedings of the IEEE International Conference on Robotics and Automation*, pages 7802–7808. IEEE, 2021. 1, 2
- [15] Alexandre Amice, Hongkai Dai, Peter Werner, Annan Zhang, and Russ Tedrake. Finding and optimizing certified, collision-

- free regions in configuration space for robot manipulators. In *International Workshop on the Algorithmic Foundations of Robotics*, pages 328–348. Springer, 2023. 2, 9
- [16] Pavel Trutman, Mohab Safey El Din, Didier Henrion, and Tomas Pajdla. Globally optimal solution to inverse kinematics of 7DOF serial manipulator. *IEEE Robotics and Automation Letters*, 7(3):6012–6019, 2022. 1, 2, 8
- [17] Jean B Lasserre. Global optimization with polynomials and the problem of moments. *SIAM Journal on optimization*, 11(3):796–817, 2001. 1, 2, 3, 10
- [18] Jean Bernard Lasserre. *An introduction to polynomial and semi-algebraic optimization*, volume 52. Cambridge University Press, 2015. 1, 2, 3, 6, 7, 10, 11
- [19] Jerrold E Marsden and Matthew West. Discrete mechanics and variational integrators. *Acta Numerica*, 10:357–514, 2001. 1, 4
- [20] Thomas Horsch, F Schwarz, and Henning Tolle. Motion planning with many degrees of freedom-random reflections at c-space obstacles. In *Proceedings of the IEEE International Conference on Robotics and Automation*, pages 3318–3323. IEEE, 1994. 2
- [21] Lydia E Kavraki, Petr Svestka, J-C Latombe, and Mark H Overmars. Probabilistic roadmaps for path planning in high-dimensional configuration spaces. *IEEE Transactions on Robotics and Automation*, 12(4):566–580, 1996.
- [22] Steven M LaValle and James J Kuffner Jr. Randomized kinodynamic planning. *International Journal of Robotics Research*, 20(5):378–400, 2001.
- [23] Karaman Sertac and Frazzoli Emilio. Sampling-based algorithms for optimal motion planning. *International Journal of Robotics Research*, 30(7):846–894, 2011. 2
- [24] Ali-Akbar Agha-Mohammadi, Suman Chakravorty, and Nancy M Amato. FIRM: Sampling-based feedback motion-planning under motion uncertainty and imperfect measurements. *International Journal of Robotics Research*, 33(2):268–304, 2014.
- [25] Geoffrey A Hollinger and Gaurav S Sukhatme. Sampling-based robotic information gathering algorithms. *International Journal of Robotics Research*, 33(9):1271–1287, 2014.
- [26] Maani Ghaffari Jadidi, Jaime Valls Miro, and Gamini Disanayake. Sampling-based incremental information gathering with applications to robotic exploration and environmental monitoring. *International Journal of Robotics Research*, 38(6):658–685, 2019. 2
- [27] Steven M LaValle. *Planning algorithms*. Cambridge university press, 2006. 2
- [28] Eugene L Lawler and David E Wood. Branch-and-bound methods: A survey. *Operations research*, 14(4):699–719, 1966. 2
- [29] Ashkan Jasour, Weiqiao Han, and Brian C. Williams. Convex Risk Bounded Continuous-Time Trajectory Planning in Uncertain Nonconvex Environments. In *Proceedings of the Robotics: Science and Systems Conference*, Virtual, July 2021. doi: 10.15607/RSS.2021.XVII.069. 2
- [30] Ashkan Jasour and Brian C Williams. Risk contours map for risk bounded motion planning under perception uncertainties. In *Proceedings of the Robotics: Science and Systems Conference*, 2019. 2, 9
- [31] Pengcheng Zhao, Shankar Mohan, and Ram Vasudevan. Optimal control of polynomial hybrid systems via convex relaxations. *IEEE Transactions on Automatic Control*, 65(5):2062–2077, 2019. 2, 3
- [32] Russ Tedrake, Ian R Manchester, Mark Tobenkin, and John W Roberts. LQR-trees: Feedback motion planning via sums-of-squares verification. *International Journal of Robotics Research*, 29(8):1038–1052, 2010. 2
- [33] Pablo A Parrilo. Semidefinite programming relaxations for semialgebraic problems. *Mathematical programming*, 96(2):293–320, 2003. 2
- [34] Grigoriy Blekherman, Pablo A Parrilo, and Rekha R Thomas. *Semidefinite optimization and convex algebraic geometry*. SIAM, 2012. 2, 7
- [35] Filip Marić, Matthew Giamou, Soroush Khoubyarian, Ivan Petrović, and Jonathan Kelly. Inverse kinematics for serial kinematic chains via sum of squares optimization. In *Proceedings of the IEEE International Conference on Robotics and Automation*, pages 7101–7107. IEEE, 2020. 2
- [36] Diego Cifuentes, Sameer Agarwal, Pablo A Parrilo, and Rekha R Thomas. On the local stability of semidefinite relaxations. *Mathematical Programming*, pages 1–35, 2020. 2
- [37] Allen Wang, Ashkan Jasour, and Brian Williams. Moment state dynamical systems for nonlinear chance-constrained motion planning. *arXiv preprint arXiv:2003.10379*, 2020. 2
- [38] Ashkan Jasour, Allen Wang, and Brian C Williams. Moment-based exact uncertainty propagation through nonlinear stochastic autonomous systems. *arXiv preprint arXiv:2101.12490*, 2021. 2, 4
- [39] Jiawang Nie. Optimality conditions and finite convergence of Lasserre’s hierarchy. *Mathematical programming*, 146(1):97–121, 2014. 2, 4
- [40] Jie Wang, Victor Magron, and Jean-Bernard Lasserre. TSSOS: A moment-SOS hierarchy that exploits term sparsity. *SIAM Journal on Optimization*, 31(1):30–58, 2021. 2, 6
- [41] Jean B Lasserre. Convergent SDP-relaxations in polynomial optimization with sparsity. *SIAM Journal on Optimization*, 17(3):822–843, 2006. 2, 6, 8, 11
- [42] Hayato Waki, Sunyoung Kim, Masakazu Kojima, and Masakazu Muramatsu. Sums of squares and semidefinite program relaxations for polynomial optimization problems with structured sparsity. *SIAM Journal on Optimization*, 17(1):218–242, 2006. 2
- [43] Jie Wang, Victor Magron, Jean B Lasserre, and Ngoc Hoang Anh Mai. CS-TSSOS: Correlative and term sparsity for large-scale polynomial optimization. *ACM Transactions on Mathematical Software*, 48(4):1–26, 2022. 2, 6
- [44] Heng Yang and Luca Carlone. Certifiably optimal outlier-robust geometric perception: Semidefinite relaxations and scalable global optimization. *IEEE Transactions on Pattern Analysis and Machine Intelligence*, 2022. 2, 4, 6
- [45] Afonso S Bandeira. A note on probably certifiably correct algorithms. *Comptes Rendus Mathematique*, 354(3):329–333, 2016. 2
- [46] Didier Henrion, Jean B Lasserre, and Carlo Savorgnan. Non-linear optimal control synthesis via occupation measures. In *Proceedings of the IEEE Conference on Decision and Control*, pages 4749–4754. IEEE, 2008. 3
- [47] Angeliki Kamoutsi, Tobias Sutter, Peyman Mohajerin Esfahani, and John Lygeros. On infinite linear programming and the moment approach to deterministic infinite horizon discounted optimal control problems. *IEEE Control Systems Letters*, 1(1):134–139, 2017.
- [48] Lujie Yang, Hongkai Dai, Alexandre Amice, and Russ Tedrake. Suboptimal controller synthesis for cart-poles and quadrotors via sums-of-squares. *arXiv preprint arXiv:2304.12533*, 2023. 3
- [49] Didier Henrion and Milan Korda. Convex computation of the region of attraction of polynomial control systems. *IEEE Transactions on Automatic Control*, 59(2):297–312, 2013. 3
- [50] Anirudha Majumdar, Ram Vasudevan, Mark M Tobenkin, and Russ Tedrake. Convex optimization of nonlinear feedback controllers via occupation measures. 33(9):1209–1230, 2014. 3
- [51] Heng Yang and Luca Carlone. One ring to rule them all: Certifiably robust geometric perception with outliers. *Proceedings of the Advances in Neural Information Processing Systems Conference*, 33:18846–18859, 2020. 4

- [52] Anthony M Bloch. Nonholonomic mechanics. In *Nonholonomic mechanics and control*, pages 207–276. Springer, 2003. 4
- [53] Jerrold E Marsden and Tudor S Ratiu. Introduction to mechanics and symmetry. 1998. 4
- [54] Elena Celledoni, Håkon Marthinsen, and Brynjulf Owren. An introduction to Lie group integrators—basics, new developments and applications. *Journal of Computational Physics*, 257:1040–1061, 2014. 4
- [55] Arieh Iserles, Hans Z Munthe-Kaas, Syvert P Nørsett, and Antonella Zanna. Lie-group methods. *Acta numerica*, 9:215–365, 2000. 4
- [56] Ayonga Hereid and Aaron D Ames. Frost: Fast robot optimization and simulation toolkit. In *Proceedings of the IEEE/RSJ International Conference on Intelligent Robots and Systems*, pages 719–726. IEEE, 2017. 5
- [57] Jerrold E Marsden, Sergey Pekarsky, and Steve Shkoller. Discrete Euler-Poincaré and Lie-Poisson equations. *Nonlinearity*, 12(6):1647, 1999. 5
- [58] Taeyoung Lee, N Harris McClamroch, and Melvin Leok. A Lie group variational integrator for the attitude dynamics of a rigid body with applications to the 3D pendulum. In *Proceedings of IEEE Conference on Control Applications*, pages 962–967. IEEE, 2005. 5
- [59] Taeyoung Lee, Melvin Leok, and N Harris McClamroch. Lie group variational integrators for the full body problem. *Computer Methods in Applied Mechanics and Engineering*, 196(29-30):2907–2924, 2007. 5
- [60] Nikolaj Nordkvist and Amit K Sanyal. A Lie group variational integrator for rigid body motion in $SE(3)$ with applications to underwater vehicle dynamics. In *Proceedings of the IEEE Conference on Decision and Control*, pages 5414–5419. IEEE, 2010. 5
- [61] Jie Wang, Victor Magron, and Jean-Bernard Lasserre. Chordal-TSSOS: a moment-sos hierarchy that exploits term sparsity with chordal extension. *SIAM Journal on Optimization*, 31(1):114–141, 2021. 6
- [62] Victor Magron and Jie Wang. TSSOS: a julia library to exploit sparsity for large-scale polynomial optimization. *arXiv preprint arXiv:2103.00915*, 2021. 6
- [63] MOSEK ApS. *MOSEK Modeling Cookbook.*, 2022. URL <https://docs.mosek.com/MOSEKModelingCookbook-letter.pdf>. 7
- [64] Erling D Andersen and Knud D Andersen. The mosek interior point optimizer for linear programming: an implementation of the homogeneous algorithm. *High performance optimization*, pages 197–232, 2000. 7
- [65] Andreas Wächter and Lorenz T Biegler. On the implementation of an interior-point filter line-search algorithm for large-scale nonlinear programming. *Mathematical programming*, 106:25–57, 2006. 7
- [66] Frank Merat. Introduction to robotics: Mechanics and control. *IEEE Journal on Robotics and Automation*, 3(2):166–166, 1987. 7
- [67] Weiqiao Han, Ashkan Jasour, and Brian Williams. Non-Gaussian risk bounded trajectory optimization for stochastic nonlinear systems in uncertain environments. In *Proceedings of the IEEE International Conference on Robotics and Automation*, pages 11044–11050. IEEE, 2022. 9
- [68] Akshay Thirugnanam, Jun Zeng, and Koushil Sreenath. Safety-critical control and planning for obstacle avoidance between polytopes with control barrier functions. In *Proceedings of the IEEE International Conference on Robotics and Automation*, pages 286–292. IEEE, 2022. 9
- [69] Ashkan Jasour and Constantino Lagoa. Convex relaxations of a probabilistically robust control design problem. In *Proceedings of the IEEE Conference on Decision and Control*, 2013. 9
- [70] Ashkan Jasour and Constantino Lagoa. Convex chance constrained model predictive control. In *Proceedings of the IEEE Conference on Decision and Control*, 2016.
- [71] Ashkan Jasour, Necdet S Aybat, and Constantino M Lagoa. Semidefinite programming for chance constrained optimization over semialgebraic sets. *SIAM Journal on Optimization*, 25(3):1411–1440, 2015. 9
- [72] Sigrid Leyendecker, Jerrold E Marsden, and Michael Ortiz. Variational integrators for constrained dynamical systems. *ZAMM-Journal of Applied Mathematics and Mechanics/Zeitschrift für Angewandte Mathematik und Mechanik: Applied Mathematics and Mechanics*, 88(9):677–708, 2008. 10
- [73] Oscar E Fernandez, Anthony M Bloch, and Peter J Olver. Variational integrators from hamiltonizable nonholonomic systems. *J. Geom. Mech*, 4(2):137–163, 2012. 10
- [74] Marin Kobilarov, Jerrold E Marsden, and Gaurav S Sukhatme. Geometric discretization of nonholonomic systems with symmetries. *Discrete and Continuous Dynamical Systems Series S*, 3(1):61–84, 2010. 10
- [75] Maani Ghaffari, Ray Zhang, Minghan Zhu, Chien Erh Lin, Tzu-Yuan Lin, Sangli Teng, Tingjun Li, Tianyi Liu, and Jingwei Song. Progress in symmetry preserving robot perception and control through geometry and learning. *Frontiers in Robotics and AI*, 9:232, 2022. 10
- [76] Heng Yang, Ling Liang, Luca Carlone, and Kim-Chuan Toh. An inexact projected gradient method with rounding and lifting by nonlinear programming for solving rank-one semidefinite relaxation of polynomial optimization. *Mathematical Programming*, pages 1–64, 2022. 10
- [77] Roger W Brockett. Dynamical systems that sort lists, diagonalize matrices, and solve linear programming problems. *Linear Algebra and its applications*, 146:79–91, 1991. 10
- [78] Anthony M Bloch, Roger W Brockett, and Tudor S Ratiu. Completely integrable gradient flows. *Communications in Mathematical Physics*, 147(1):57–74, 1992.
- [79] William Clark, Maani Ghaffari, and Anthony Bloch. Non-parametric continuous sensor registration. *Journal of Machine Learning Research*, 22(271):1–50, 2021.
- [80] Sangli Teng, William Clark, Anthony Bloch, Ram Vasudevan, and Maani Ghaffari. Lie algebraic cost function design for control on Lie groups. In *Proceedings of the IEEE Conference on Decision and Control*, pages 1867–1874. IEEE, 2022.
- [81] Sangli Teng, Dianhao Chen, William Clark, and Maani Ghaffari. An error-state model predictive control on connected matrix Lie groups for legged robot control. In *Proceedings of the IEEE/RSJ International Conference on Intelligent Robots and Systems*, pages 8850–8857. IEEE, 2022. 10